

SMAP : Self-supervised Motion Adaptation for Physically Plausible Humanoid Whole-body Control

Haoyu Zhao^{*1,2}, Sixu Lin^{*3}, Qingwei Ben^{2,4}, Minyue Dai⁵, Hao Fei⁶,
Jingbo Wang², Hua Zou^{†1}, Junting Dong^{†2}

¹School of Computer Science, Wuhan University ²Shanghai Artificial Intelligence Laboratory

³Harbin Institute of Technology (Shenzhen) ⁴The Chinese University of Hong Kong

⁵Fudan University ⁶National University of Singapore

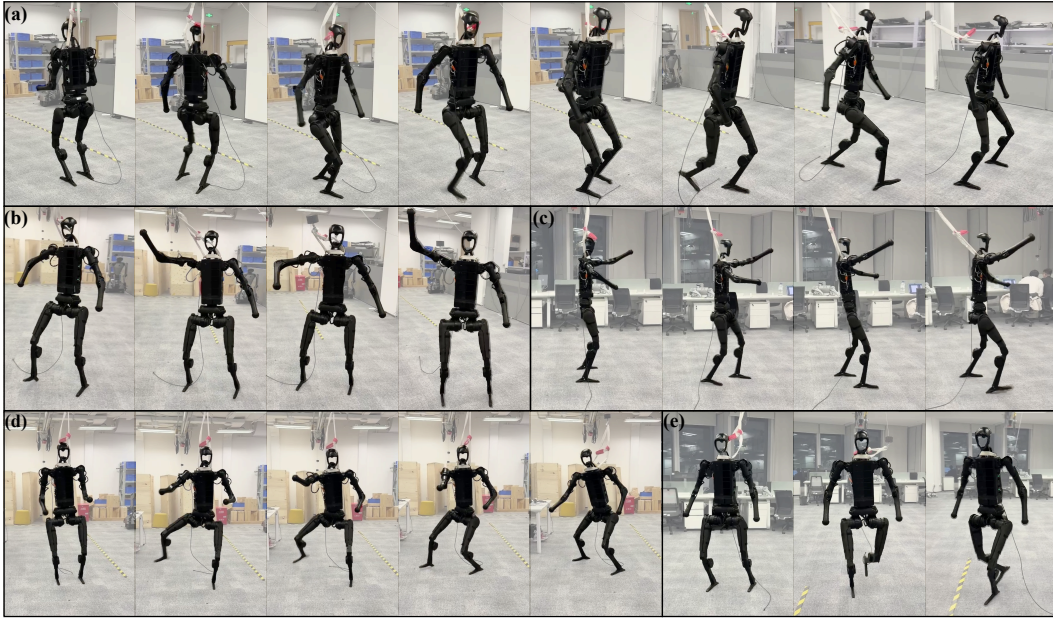


Figure 1: Our framework enables humanoid robot execute various expressive whole-body motions. The robot can (a) turn around and walk forward, (b) wave hello, (c) swing arms while advancing, (d) jump on one leg, (e) walk fast.

Abstract

This paper presents a novel framework that enables real-world humanoid robots to maintain stability while performing human-like motion. Current methods train a policy which allows humanoid robots to follow human body using the massive retargeted human data via reinforcement learning. However, due to the heterogeneity between human and humanoid robot motion, directly using retargeted human motion reduces training efficiency and stability. To this end, we introduce **SAMP**, a novel whole-body tracking framework that bridges the gap between human and humanoid action spaces, enabling accurate motion mimicry by humanoid robots. The core idea is to use a vector-quantized periodic autoencoder to capture generic atomic behaviors and adapt human motion into physically plausible humanoid motion. This adaptation accelerates training convergence and improves stability

* Equal contributions.

†Corresponding Author.

when handling novel or challenging motions. We then employ a privileged teacher to distill precise mimicry skills into the student policy with a proposed decoupled reward. We conduct experiments in simulation and real world to demonstrate the superiority stability and performance of SAMP over SOTA methods, offering practical guidelines for advancing whole-body control in humanoid robots. Our project page is at <https://smap-project.github.io/>.

1 Introduction

Humanoid robots, with their human-like morphology, have long been a focal point in robotics due to their potential to perform diverse daily tasks [53, 29]. Designed for human environments, tools, and interactions, human-sized humanoids serve as ideal platforms for general-purpose robotics, naturally adapting to tasks suited for humans. However, achieving this versatility requires precise and robust whole-body control, enabling humanoid robots to coordinate high-degree-of-freedom movements for safe and effective interaction with their surroundings.

Traditional approaches, which decompose the problem into perception, planning, and tracking while modularizing arm and leg control separately [8, 13, 27], are time-consuming to design, limited in scope. These limitations make it challenging to scale humanoids to the diverse range of tasks and environments in which they are expected to operate. Human motion capture datasets [33, 18, 38, 5] provide a rich source of reference motion, enabling the imitation of everyday human activities [54, 52]. With the growing availability of large-scale human motion datasets, recent approaches [15, 6, 20, 21, 25, 32, 19] leverage Reinforcement Learning (RL) to track and mimic re-targeted human motion, allowing humanoid robots to learn versatile behaviors. For example, Human-Plus [15] presents a system that enables humanoids to learn and imitate human motion and skills in real time using RL. However, a major challenge lies in the significant heterogeneity of re-targeted human motion data. Given that humanoid robots and humans have entirely distinct action spaces, directly using human motion data as an imitation goal often results in physically implausible motion, leading to low training efficiency and instability. This poses a compelling research question: *How to formulate imitation goals that ensure both physical plausibility and human-like motion for humanoid robots?*

To address the aforementioned challenges, we propose **SAMP**, an effective framework for **Self-supervised Motion Adaptation**, enabling **Physically plausible** whole-body control for humanoid robots. Unlike previous methods that operate within the heterogeneous re-targeted human action space, we train and perform inference within the physically plausible action space for humanoid robots. Specifically, we introduce **Humanoid-Adapter**, a vector-quantized periodic autoencoder that maps human motion to humanoid robot actions. By encoding human motion sequences into a shared codebook, we decompose motion into generic atomic behaviors and then decoding them into corresponding motion for humanoid robot, our method enables an efficient transformation between human and robot movements, as shown in Fig. 2. The adapted motion, serving as an imitation goal, significantly improves policy stability and accelerates training convergence. Additionally, through teacher-student distillation and a decoupled reward that separately optimizes upper and lower body dynamics, we further enhance both motion performance and stability. Extensive experiments on humanoid platforms, Unitree H1, demonstrate that our method achieves superior performance in full-body tracking accuracy and velocity tracking while maintaining stability in dynamic environments. In summary, our work makes the following contributions:

- We propose a novel framework for training a robust whole-body control policy that addresses the heterogeneity between human and humanoid action spaces.

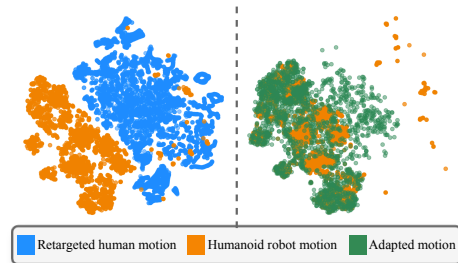


Figure 2: **t-SNE visualization** of the distribution of **re-targeted human motion**, **humanoid robot motion** (recorded within the simulator), and **motion adapted by Humanoid-Adapter** on the CMU MoCap dataset [5].

- We propose a vector-quantized periodic autoencoder that adapts human motion into physically plausible motion for training and inference.
- Experiments in simulation and real world validate our method’s superior motion imitation and stability.

2 Related Work

2.1 Humanoid Whole-Body Control

Humanoid robots have great potential to unlock the full capabilities of humanoid systems, but remains a long-standing challenge due to their high degrees of freedom (DoF) and non-linearity [17, 22]. Traditional approaches often rely on human motion capture suits [10, 11, 3], haptic feedback devices [4, 37, 42], and dynamics modeling and control [9, 35, 42, 48, 51]. Recent advances in sim-to-real reinforcement learning (RL) and sim-to-real transfer show promising results in enabling complex whole-body skills for humanoid robots such as walking [2, 21, 24, 7, 12, 14, 16, 49, 40, 41], jumping [19], parkour [56], dancing [15, 6, 20], and hopping [25]. For example, H2O [21] presents an RL-based teleoperation framework using a third-person RGB camera to capture the human teleoperator’s full-body keypoints. Exbody [6] focuses on imitating upper-body reference motion (retargeted from human data) while allowing the legs to robustly follow a given velocity. However, these methods directly use retargeted human motion, which leads to inefficient training and unstable performance due to the significant heterogeneity between human and humanoid robot motion. To address this, we propose Humanoid-Adapter that adapt human motion into the humanoid robot action space, facilitating more efficient and stable learning.

2.2 Motion Retargeting

Traditional approaches [28, 46] often focus on optimizing low-level motion representations or transferring motions to new skeletons, rather than learning a shared representation. This is a common approach used in previous humanoid whole-body control methods [15, 6, 20, 21, 25, 32, 19]. Recent deep learning advances [47, 1, 31] shift towards learning a common cross-character latent space. These methods still require paired data or rely on skeletons for effective learning and auxiliary loss application. For instance, HumanConQuad [26] introduces a human motion-based control interface for quadrupedal robots. Our method achieves a similar effect by leveraging unpaired human motion and RL-generated humanoid robot motion, aligning them to produce physically plausible motion.

2.3 Motion Manifold Learning

Motion manifold learning has the primary goal of comprehending the fundamental structures inherent in human movement and dynamics [30, 45]. Its distinctive ability to generate human movement patterns presents numerous opportunities to comprehend intrinsic motion dynamics, manage nonlinear relationships in motion data, and acquire contextual and hierarchical representations [50, 39]. Holden et al.[23] generate character movements by mapping high-level parameters to the human motion manifold, enabling diverse motion. Recently, DeepPhase[45] propose Periodic Autoencoder to learn a low-dimensional motion manifold. With vector quantized periodic autoencoder, we learn a shared phase manifold for human and humanoid robot. The discrete amplitude vectors serve as a narrow bottleneck to regularize unsupervised learning of semantic motion clusters.

3 Preliminaries

Goal-conditioned Reinforcement Learning. In this work, we train a goal-conditioned policy π to achieve whole-body control by imitating reference motion. The learning process is formulated as a Markov Decision Process (MDP), defined by the tuple $\mathcal{M} = \langle \mathcal{S}, \mathcal{A}, \mathcal{T}, \mathcal{R}, \gamma \rangle$, which includes the state space \mathcal{S} , action space \mathcal{A} , transition dynamics \mathcal{T} , reward function \mathcal{R} , and discount factor γ . The state $s_t \in \mathcal{S}$ and transition dynamics \mathcal{T} are determined by the physics simulation [34], which computes the action a_t based on the policy π . The state s_t consists of proprioception s_t^p and a goal state s_t^g . The proprioception captures the robot’s internal dynamics, while the goal state s_t^g provides task-specific guidance. The reward function is defined as $r_t = \mathcal{R}(s_t^p, s_t^g)$, encouraging the policy π

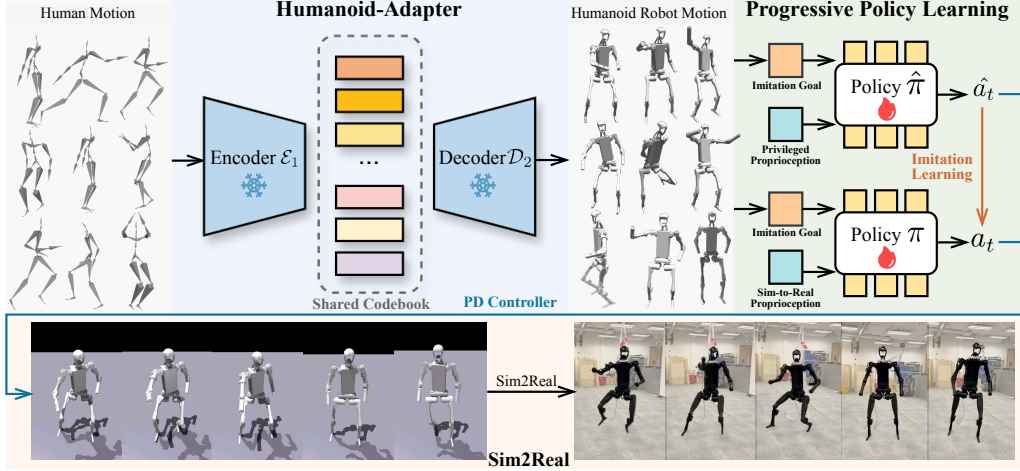



Figure 3: **Pipeline of SMAP** . Given human motion, we use the proposed **Humanoid-Adapter** (details shown in Fig. 9), pre-trained (❄️) to adapt human motion into corresponding, physically plausible humanoid robot motion. Our sim-to-real policy (❤️) is distilled via imitation learning from an RL-trained privileged teacher policy that leverages privileged information with proposed decoupled reward. The policy is transferred to the real world.

to maximize long-term rewards. To optimize the policy π , we employ Proximal Policy Optimization (PPO)[44], maximizing the objective $\mathbb{E} \left[\sum_{t=1}^T \gamma^{t-1} r_t \right]$.

The action space for humanoid robot is represented as $a_t \in \mathbb{R}^{n \times 3}$, where n is the number of actuated degrees of freedom (DoFs). Each DoF is controlled by a proportional-derivative (PD) controller, and the action a_t specifies the PD target. Our humanoid model follows the kinematic structure of the Unitree H1 robot which has 23 DoFs.

4 Method

We introduce **SMAP**, an effective sim-to-real framework for robust whole-body humanoid control, as illustrated in Fig. 3. To deal with the the heterogeneity between human and humanoid robot motion, we propose **Humanoid-Adapter** to adapt human motion action space into physically plausible humanoid robot action space. We then propose **Progressive Control Policy Learning**, which leverages teacher-student distillation to incorporate privileged inputs and employs a decoupled reward to enhance both the performance and stability of the humanoid robot’s motion.

4.1 Humanoid-Adapter

To transform human motion action space into humanoid robot motion action space, we pre-train Humanoid-Adapter, built upon the Periodic Autoencoder (PAE) [45], to learn a continuous phase manifold, align motion, and cluster semantically similar movements, as shown in Fig. 4.

Inspired by [30, 45], we aim to learn a generative phase representation for both human and humanoid robot motion, enabling indefinite motion synthesis while preserving temporal coherence and dynamic consistency. To build a humanoid robot motion dataset, \mathcal{S}^r , we train a goal-conditioned RL-based policy [6] and record the humanoid robot’s motion data within the simulator. Using both the humanoid robot motion dataset \mathcal{S}^r and the human motion dataset [5] \mathcal{S}^h , we learn a shared phase manifold for human and humanoid robot characters without any supervision.

Phase Manifold. The Humanoid-Adapter models the latent variational distribution using the phase parameter, which is extracted from the latent motion curve, referred to as the variational phase manifold. This phase manifold is highly structured, capturing key motion characteristics such as timing, local periodicity, and transitions, which are crucial for learning motion features [30]. Given

an input motion sequence d , our goal is to map each frame d_i to a point p on the phase manifold \mathcal{P} :

$$p = \Psi(\alpha, \phi) = \alpha^0 \sin(2\pi\phi) + \alpha^1 \cos(2\pi\phi), \quad (1)$$

where ϕ is the phase parameter, and α is a vector amplitude composed of two components: α^0 and α^1 , representing its first and second halves, respectively. To learn a discrete amplitude space, we employ the vector quantization to cluster the vector amplitude α into a learnable codebook \mathcal{C} , represented as:

$$\mathcal{C} = (c_1, c_2, c_3 \dots c_n), \quad (2)$$

where n is the space size and each c_i is a vector embedding that represents a atomic behavior. Motion with similar characteristics are placed close to each other.

Structure of Humanoid-Adapter. Humanoid-Adapter enables learning a shared phase manifold for both human and humanoid robot motion, without the need for supervision. This is achieved by leveraging the discrete structure, ensuring that semantically similar motion are clustered along the same curve of the manifold.

We use an encoder to predict the amplitude α , phase ϕ and frequency f , with vector quantization applied to select the nearest amplitude from a finite codebook \mathcal{C} . We then assume the amplitude α and phase ϕ hold for the whole input motion sequence and extrapolate the phase linearly with the predicted frequency to the whole sequence. We calculate the embeddings using Eq. 1 with extrapolated phases ϕ and amplitudes α . A decoder is then used to reconstruct the input motion sequence d from the predicted embedding.

As shown in Fig. 4, to align human and humanoid robot motion, a phase manifold is learned using a shared codebook \mathcal{C} . We train two VQ-PAEs on two datasets: the human motion dataset \mathcal{S}^h and the humanoid robot motion dataset \mathcal{S}^r , each with distinct skeletal structures. The loss function for training these networks can be expressed as follows:

$$\mathcal{L} = \|s^r - \hat{s}^r\|_2 + \|s^h - \hat{s}^h\|_2, \quad (3)$$

where $s^r \in \mathcal{S}^r$, $s^h \in \mathcal{S}^h$, and \hat{s}^r , \hat{s}^h are adapted motion. Directly optimizing Eq. 3 may cause imbalanced codebook utilization, a common issue in VQ-VAE frameworks due to codebook underutilization. We adapt CVQ-VAE’s reinitialization [55] to maintain active embeddings across both motion domains. This method dynamically replaces underused codes during training, ensuring balanced representation learning for both data \mathcal{S}^r and \mathcal{S}^h .

During inference, we use the encoder \mathcal{E}_1 and the decoder \mathcal{D}_2 to adapt human motion into humanoid robot motion. The proposed Humanoid-Adapter effectively bridges the domain gap between human motion and physically executable humanoid robot motion, ensuring kinematically feasible and dynamically stable motion, as shown in Fig. 2.

4.2 Progressive Control Policy Learning

During real-world whole-body control of a humanoid robot, much of the information (*e.g.* global linear/angular velocity, positions of each link, and physical properties) which is available in simulation, is not accessible. To address this, our control policy employs a progressive two-stage teacher-student training. In the first stage, the teacher policy is trained using privileged information that can only be obtained in simulation. In the second stage, we replace this privileged information with real-world observations, and distill the teacher policy into a student policy.

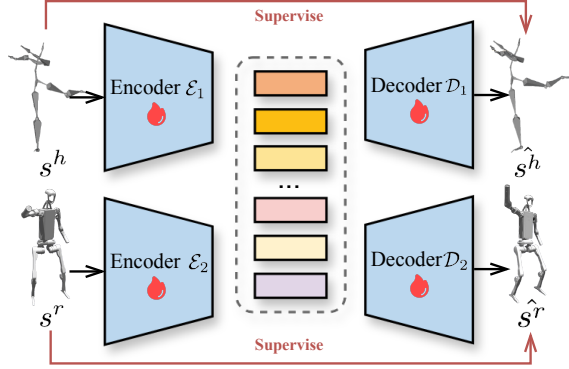


Figure 4: **Humanoid-Adapter.** To align heterogeneous human motion \mathcal{S}^h and humanoid robot motion \mathcal{S}^r , we train two VQ-PAEs (🔥) on them to learn a shared phase manifold using a codebook.

| Method | Trained Motion Sample | | | | Novel Motion Sample | | | |
|---------------------------------------|-----------------------|------------------------|------------------------|-------------------|----------------------|------------------------|------------------------|-------------------|
| | $E_{vel} \downarrow$ | $E_{mpkpe} \downarrow$ | $E_{mpjpe} \downarrow$ | $fail \downarrow$ | $E_{vel} \downarrow$ | $E_{mpkpe} \downarrow$ | $E_{mpjpe} \downarrow$ | $fail \downarrow$ |
| Privileged policy | 0.1002 | 0.0531 | 0.0888 | 798 | 0.1923 | 0.0732 | 0.1121 | 199 |
| HumanPlus [15] | 0.3103 | 0.1011 | 0.1989 | 3009 | 0.4299 | 0.1598 | 0.2612 | 633 |
| H2O [21] | 0.2333 | 0.0831 | 0.1989 | 2762 | 0.3613 | 0.1385 | 0.2212 | 501 |
| OmniH2O [20] | 0.1791 | 0.0619 | 0.1250 | 1899 | 0.2591 | 0.0912 | 0.1481 | 387 |
| Exbody [6] | 0.2160 | 0.0766 | 0.1783 | 2264 | 0.3002 | 0.1070 | 0.1868 | 432 |
| Exbody [†] [6] | 0.2285 | 0.0770 | 0.1592 | 2322 | 0.3239 | 0.1099 | 0.1749 | 489 |
| Exbody + AMP [36] | 0.2499 | 0.0732 | 0.1531 | 1993 | 0.3487 | 0.1002 | 0.1604 | 412 |
| Exbody + Humanoid-Adapter | - | - | - | - | 0.2998 | 0.0999 | 0.1632 | 361 |
| SAMP | 0.1698 | 0.0608 | 0.1181 | 1731 | 0.2331 | 0.0893 | 0.1458 | 266 |
| SAMP w/o Humanoid-Adapter | 0.1743 | 0.0612 | 0.1221 | 1851 | 0.2465 | 0.0921 | 0.1442 | 392 |
| SAMP w/o teacher-student distillation | 0.2038 | 0.0732 | 0.1521 | 1751 | 0.2765 | 0.0941 | 0.1641 | 389 |
| SAMP w/o progressive | 0.1712 | 0.0610 | 0.1191 | 1889 | 0.2387 | 0.0914 | 0.1468 | 299 |
| SAMP w/o decoupled reward | 0.1739 | 0.0659 | 0.1283 | 1775 | 0.2389 | 0.0903 | 0.1499 | 291 |

Table 1: **Quantitative Comparisons and Ablation Study.** Simulation-based motion imitation evaluation of our method and state-of-the-art (SOTA) approaches on the CMU MoCap dataset [5] for the Unitree H1 robot.

Curriculum-based Teacher Policy Training. The teacher policy $\hat{\pi}$ takes privileged proprioception and imitation goals as inputs and outputs the action \hat{a}_t . The privileged information $s_t^{privileged}$ includes ground-truth states of the humanoid robot and environment (e.g., root velocity, body link positions, and physical properties). For details on privileged information, please refer to the Supp.Mat.

The training process follows a progressive curriculum strategy, initially leveraging reconstructed, physically plausible humanoid robot motion data (generated by the Humanoid-Adapter) to stabilize policy learning, while gradually introducing and encouraging exploration of retargeted human motion data. This curriculum learning approach not only ensures convergence stability but also expands the policy’s action space.

Student Policy Distilling. In this stage, we remove privileged proprioception and leverage sim-to-real proprioception (a longer history of observations) to train the student policy. The policy is supervised using the teacher policy’s action \hat{a}_t with loss followed:

$$\mathcal{L}_{distill} = \|a_t - \hat{a}_t\|_2. \quad (4)$$

To train the student policy, we follow the DAgger [43] framework, rolling out the student policy π in the simulation environment to collect training data. At each visited state, the teacher policy $\hat{\pi}$ generates an oracle action as the supervision signal. The student policy π is iteratively refined by minimizing the loss $\mathcal{L}_{distill}$.

Decoupled Reward Design Our reward function is designed to improve both performance and stability of the humanoid robot’s motion. It includes tracking rewards for velocity, direction, orientation of the root, keypoint, and joint position. To balance precision and stability, we decouple the upper and lower body: higher weight is assigned to the upper body for precision, while lower weight is given to the lower body to prioritize balance [3]. Regularization terms are also included to enhance stability and generalization. For more detailed tracking rewards, please refer to the Supp.Mat.

5 Experiments

5.1 Implementation Details

We conduct our experiments in IsaacGym [34] simulator. During training, 4096 environments are simulated in parallel on a NVIDIA RTX 4090 GPU.

5.2 Dataset

Following Exbody [6], we selectively use a portion of the CMU MoCap dataset [5], excluding motion involving physical interactions with other individuals, heavy objects, or rough terrain. This diversity

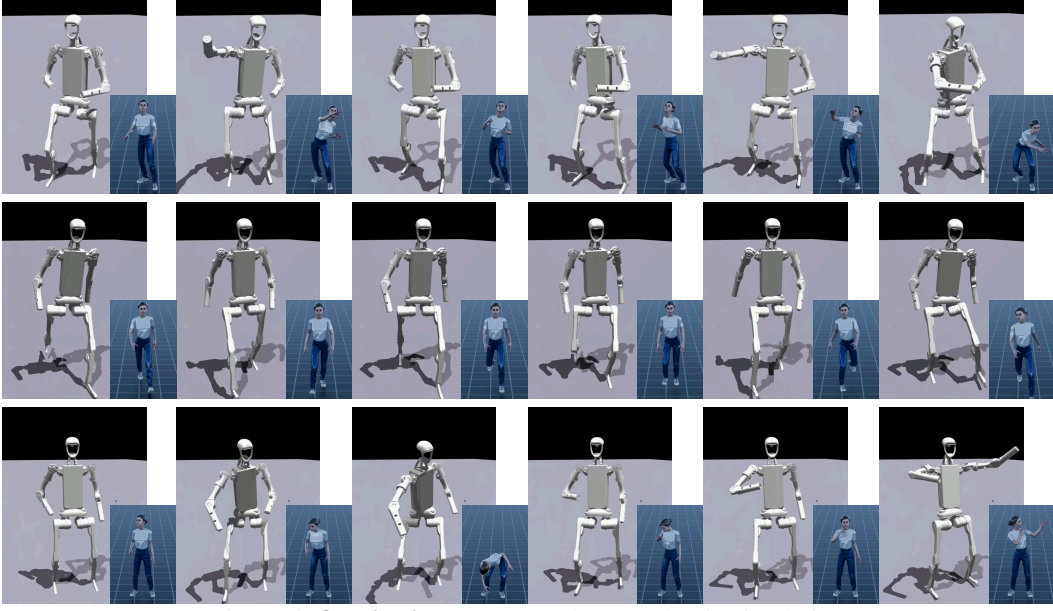


Figure 5: **Qualitative results** on the H1 robot in simulation.

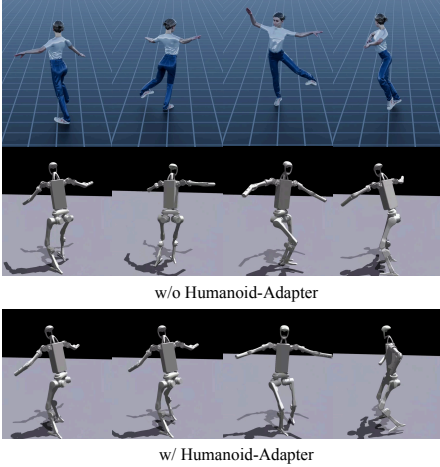


Figure 6: **Ablation study**. Visualization performance in the simulation on challenging motion sample.

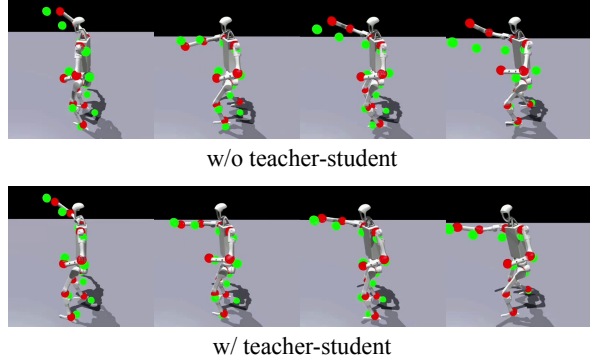


Figure 7: **Ablation study** of teacher-student distillation. The **green** points represent the imitation goal, while the **red** points correspond to the DOF position.

not only enhances the expressiveness of humanoid motion but also improves locomotion stability in unseen scenarios. To further evaluate robustness and generalization, we also test on **novel motion** from the CMU dataset that are not used during training.

5.3 Evaluation Metrics

We evaluate the policy’s performance using several metrics computed across all motion sequences in the dataset. **The mean linear velocity error** (E_{vel}) measures the discrepancy between the robot’s root linear velocity and the demonstration, reflecting velocity tracking accuracy. **The mean per key point position error** (E_{mpkpe}) and **the mean per joint position error** (E_{mpjpe}) evaluate motion accuracy, with E_{mpkpe} assessing keypoint tracking and E_{mpjpe} capturing joint tracking accuracy. **Failure** (*fail*) counts the number of failure terminations across all motion sequences. Lower failure rates suggest greater robustness and control consistency across diverse motions.



Figure 8: **Qualitative result** on the H1 robot in real world.

5.4 Comparison with SOTA Methods

We evaluate our method on motion tracking in simulation across Unitree H1, comparing it with three state-of-the-art methods: HumanPlus [15], H2O [21], OmniH2O [20], and Exbody [6]. This teacher policy (privileged policy) leverages all privileged environment information as mentioned in its observations. For a fair comparison, we reimplement the H2O [21] and OmniH2O [20] using global keypoint tracking and the same observation space. Since Exbody [6] only tracks upper-body motion, we introduce a whole-body tracking variant (Exbody[†]) to enable direct comparison. This version tracks full-body movements based on human motion data. Exbody + AMP [36] uses an AMP reward to encourage the policy’s transitions to be similar to those in the retargeted dataset.

We evaluate our method on the retargeted CMU MoCap dataset [5] in simulation, following Exbody [6], as shown in Tab. 1. Our method achieves high full-body tracking accuracy and excels in velocity tracking, outperforming other state-of-the-art methods. This improvement stems from the teacher-student distillation, where distilling privileged information into historical observations enables the student policy to track velocity more effectively. Additionally, our method has the fewest failure cases, demonstrating its robustness. This is largely attributed to the proposed Humanoid-Adapter, which transforms human motion into physically plausible motion, making it easier for the humanoid robot to track while maintaining stability. Notably, *the motion adapted by the proposed Humanoid-Adapter also enhances the stability of other RL-based methods* (Exbody + Humanoid-Adapter), further demonstrating its strong generalizability.

Fig.5 presents qualitative results in simulation, where the humanoid robot successfully replicates various human motions, such as fast walking and squatting, while maintaining stability. Additionally, Fig.8 showcases real-world experimental results, further demonstrating the robustness of our policy in real-world settings.

5.5 Ablation Study

In this section, we conduct experiments to evaluate the effectiveness of proposed modules in Tab. 1

Humanoid-Adapter. To evaluate the impact of Humanoid-Adapter, we replace it with directly retargeted human motion (SAMP w/o Humanoid-Adapter) during both training and inference. Since retargeted human motion may not always be physically plausible, the tracking performance de-

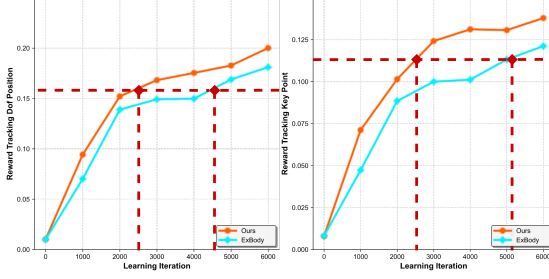


Figure 9: **Training Curves Comparison** between SAMP and Exbody[†]

| | $E_{vel} \downarrow$ | $E_{mpkpe} \downarrow$ | $E_{mpjpe} \downarrow$ | $fail \downarrow$ |
|-------------------------------------|----------------------|------------------------|------------------------|-------------------|
| Codebook Size C | | | | |
| 16 | 0.1732 | 0.0611 | 0.1192 | 1798 |
| 32 | 0.1698 | 0.0608 | 0.1181 | 1731 |
| 64 | 0.1698 | 0.0610 | 0.1190 | 1799 |
| History Length | | | | |
| 0 | 0.2831 | 0.0751 | 0.1591 | 1973 |
| 5 | 0.1751 | 0.0623 | 0.1289 | 1787 |
| 10 | 0.1698 | 0.0608 | 0.1181 | 1731 |
| 32 | 0.1781 | 0.0608 | 0.1188 | 1719 |

Figure 10: **Ablation Study Results** (Best values in bold)

grades significantly under novel and challenging motion samples, ultimately reducing robot stability. Humanoid-Adapter adapts complex motion into more robot-friendly forms, enabling more stable and accurate motion tracking as shown in Fig. 6.

With more physically plausible motion as the imitation goal, our method also accelerates training convergence, leading to significantly faster improvements in tracking DOF positions and keypoint rewards compared to Exbody[†]. Specifically, our approach reaches the same level of performance as Exbody[†] in nearly half the iterations—achieving comparable results in just 2500 iterations, whereas Exbody[†] requires over 4500 iterations.

Progressive Control Policy Learning. We first analyze the impact of teacher-student distillation. Without this training (SAMP w/o teacher-student distillation), tracking accuracy decreases significantly. This is primarily due to the lack of privileged velocity guidance, which makes it challenging for the single-stage RL policy to learn velocity directly from historical data. As shown in Fig. 7, the policy without teacher-student distillation demonstrates lower tracking precision. We then examine the effectiveness of the proposed progressive learning. We find that directly using the final weight for policy training (SAMP w/o progressive) yields worse results. This is because gradually allowing the model to learn retargeted motion is crucial for improving learning performance.

Decoupled Reward. We observe that the control policy employing the decoupled reward demonstrates significantly higher precision in tracking motion targets and fewer failures. This improvement is due to the upper body’s greater need for precision in task execution, while the lower body is prioritized for overall balance rather than strict positional accuracy.

Hyperparameters of SAMP. Choosing an appropriate codebook size is critical for our framework, as a small codebook size fails to capture the diverse semantics, and a large codebook reduces semantic alignment accuracy. As shown in Tab. 10, a codebook size of 32 yields the best performance.

We also test student policies trained with varying history lengths in Tab. 10. Without additional history, the policy struggles to learn effectively. History length of 10 produces the best results, which we use in our experiments. Longer history lengths increase the difficulty of fitting privileged information, ultimately reducing tracking performance.

6 Conclusion

This paper introduces **SMAP**, a novel sim-to-real framework for whole-body humanoid control. Different from previous methods, we use a network to map human motion into the humanoid robot’s action space for training and inference. For superior disentanglement, we propose a vector-quantized periodic autoencoder to bridge the gap between human motion and humanoid robots. Then, we propose Progressive Control Policy Learning, leveraging teacher-student distillation and employing a decoupled reward that separately optimizes upper and lower body dynamics. Extensive experiments in simulation and real world demonstrate that our SAMP achieves superior full-body tracking accuracy while maintaining stability.

Limitation and future work. One limitation of SAMP is the lack of explicit joint correspondence, which may cause minor mismatches in motion alignment. By sampling motion in action space of

humanoid robot, Humanoid-Adapter can be a data augmentation tool to generate reliable motion, offering a promising avenue for future research.

References

- [1] K. Aberman, P. Li, D. Lischinski, O. Sorkine-Hornung, D. Cohen-Or, and B. Chen. Skeleton-aware networks for deep motion retargeting. *ACM Transactions on Graphics (TOG)*, 39(4):62–1, 2020. 3
- [2] A. Agarwal, A. Kumar, J. Malik, and D. Pathak. Legged locomotion in challenging terrains using egocentric vision. In *Proc. of Conf. on Robot Learning*, pages 403–415, 2023. 3
- [3] Q. Ben, F. Jia, J. Zeng, J. Dong, D. Lin, and J. Pang. Homie: Humanoid loco-manipulation with isomorphic exoskeleton cockpit. *arXiv preprint arXiv:2502.13013*, 2025. 3, 6
- [4] A. Brygo, I. Sarakoglou, N. Garcia-Hernandez, and N. Tsagarakis. Humanoid robot teleoperation with vibrotactile based balancing feedback. In *Haptics: Neuroscience, Devices, Modeling, and Applications: 9th International Conference, EuroHaptics 2014, Versailles, France, June 24-26, 2014, Proceedings, Part II 9*, pages 266–275. Springer, 2014. 3
- [5] Carnegie Mellon University. Carnegie-Mellon mocap database. <http://mocap.cs.cmu.edu/>, Mar 2007. [Online]. 2, 4, 6, 8
- [6] X. Cheng, Y. Ji, J. Chen, R. Yang, G. Yang, and X. Wang. Expressive whole-body control for humanoid robots. In *Proc. of Robotics: Science and Systems*, 2024. 2, 3, 4, 6, 8
- [7] X. Cheng, A. Kumar, and D. Pathak. Legs as manipulator: Pushing quadrupedal agility beyond locomotion. In *Proc. of IEEE Int. Conf. on Robotics and Automation*, pages 5106–5112. IEEE, 2023. 3
- [8] J. Chestnutt, M. Lau, G. Cheung, J. Kuffner, J. Hodgins, and T. Kanade. Footstep planning for the honda asimo humanoid. In *Proc. of IEEE Int. Conf. on Robotics and Automation*, pages 629–634, 2005. 2
- [9] B. Dariush, M. Gienger, B. Jian, C. Goerick, and K. Fujimura. Whole body humanoid control from human motion descriptors. In *Proc. of IEEE Int. Conf. on Robotics and Automation*, pages 2677–2684. IEEE, 2008. 3
- [10] K. Darvish, Y. Tirupachuri, G. Romualdi, L. Rapetti, D. Ferigo, F. J. A. Chavez, and D. Pucci. Whole-body geometric retargeting for humanoid robots. In *IEEE-RAS 19th International Conference on Humanoid Robots (Humanoids)*, pages 679–686. IEEE, 2019. 3
- [11] A. D. Dragan, K. C. Lee, and S. S. Srinivasa. Legibility and predictability of robot motion. In *ACM/IEEE International Conference on Human-Robot Interaction*, pages 301–308. IEEE, 2013. 3
- [12] A. Escontrela, X. B. Peng, W. Yu, T. Zhang, A. Iscen, K. Goldberg, and P. Abbeel. Adversarial motion priors make good substitutes for complex reward functions. In *Proc. of IEEE/RSJ Int. Conf. on Intelligent Robots and Systems*, pages 25–32. IEEE, 2022. 3
- [13] S. Feng, E. Whitman, X. Xinjilefu, and C. G. Atkeson. Optimization based full body control for the atlas robot. In *IEEE-RAS International Conference on Humanoid Robots*, pages 120–127, 2014. 2
- [14] Z. Fu, X. Cheng, and D. Pathak. Deep whole-body control: learning a unified policy for manipulation and locomotion. In *Proc. of Conf. on Robot Learning*, pages 138–149. PMLR, 2023. 3
- [15] Z. Fu, Q. Zhao, Q. Wu, G. Wetzstein, and C. Finn. HumanPlus: Humanoid shadowing and imitation from humans. In *Proc. of Conf. on Robot Learning*, 2024. 2, 3, 6, 8
- [16] Y. Fuchioka, Z. Xie, and M. Van de Panne. Opt-mimic: Imitation of optimized trajectories for dynamic quadruped behaviors. In *Proc. of IEEE Int. Conf. on Robotics and Automation*, pages 5092–5098. IEEE, 2023. 3
- [17] J. W. Grizzle, J. Hurst, B. Morris, H.-W. Park, and K. Sreenath. Mabel, a new robotic bipedal walker and runner. In *American Control Conference*, pages 2030–2036. IEEE, 2009. 3
- [18] C. Guo, S. Zou, X. Zuo, S. Wang, W. Ji, X. Li, and L. Cheng. Generating diverse and natural 3d human motions from text. In *Proc. of IEEE Conf. on Computer Vision and Pattern Recognition*, pages 5152–5161, 2022. 2
- [19] T. He, J. Gao, W. Xiao, Y. Zhang, Z. Wang, J. Wang, Z. Luo, G. He, N. Sobanbab, C. Pan, et al. Asap: Aligning simulation and real-world physics for learning agile humanoid whole-body skills. *arXiv preprint arXiv:2502.01143*, 2025. 2, 3
- [20] T. He, Z. Luo, X. He, W. Xiao, C. Zhang, W. Zhang, K. Kitani, C. Liu, and G. Shi. Omnih2o: Universal and dexterous human-to-humanoid whole-body teleoperation and learning. In *Proc. of Conf. on Robot Learning*, 2024. 2, 3, 6, 8
- [21] T. He, Z. Luo, W. Xiao, C. Zhang, K. Kitani, C. Liu, and G. Shi. Learning human-to-humanoid real-time whole-body teleoperation. In *Proc. of IEEE/RSJ Int. Conf. on Intelligent Robots and Systems*, 2024. 2, 3, 6, 8
- [22] K. Hirai, M. Hirose, Y. Haikawa, and T. Takenaka. The development of honda humanoid robot. In *Proc. of IEEE Int. Conf. on Robotics and Automation*, volume 2, pages 1321–1326. IEEE, 1998. 3
- [23] D. Holden, J. Saito, and T. Komura. A deep learning framework for character motion synthesis and editing. *ACM Transactions on Graphics (TOG)*, 35(4):1–11, 2016. 3

- [24] H. Ito, K. Yamamoto, H. Mori, and T. Ogata. Efficient multitask learning with an embodied predictive model for door opening and entry with whole-body control. *Science Robotics*, 7(65):eaax8177, 2022. 3
- [25] M. Ji, X. Peng, F. Liu, J. Li, G. Yang, X. Cheng, and X. Wang. Exbody2: Advanced expressive humanoid whole-body control. *arXiv preprint arXiv:2412.13196*, 2024. 2, 3
- [26] S. Kim, M. Sorokin, J. Lee, and S. Ha. Humanconquad: human motion control of quadrupedal robots using deep reinforcement learning. In *SIGGRAPH Asia 2022 Emerging Technologies*, pages 1–2. 2022. 3
- [27] S. Kuindersma, R. Deits, M. Fallon, A. Valenzuela, H. Dai, F. Permenter, T. Koolen, P. Marion, and R. Tedrake. Optimization-based locomotion planning, estimation, and control design for the atlas humanoid robot. *Autonomous robots*, 40:429–455, 2016. 2
- [28] J. Lee and S. Y. Shin. A hierarchical approach to interactive motion editing for human-like figures. In *Proceedings of the 26th annual conference on Computer graphics and interactive techniques*, pages 39–48, 1999. 3
- [29] H. Li, Q. Zhao, H. Xu, X. Jiang, Q. Ben, F. Jia, H. Zhao, L. Xu, J. Zeng, H. Wang, et al. Teleopbench: A simulator-centric benchmark for dual-arm dexterous teleoperation. *arXiv preprint arXiv:2505.12748*, 2025. 2
- [30] P. Li, S. Starke, Y. Ye, and O. Sorkine-Hornung. Walkthedog: Cross-morphology motion alignment via phase manifolds. In *ACM SIGGRAPH 2024 Conference Papers*, pages 1–10, 2024. 3, 4
- [31] T. Li, J. Won, A. Clegg, J. Kim, A. Rai, and S. Ha. Ace: Adversarial correspondence embedding for cross morphology motion retargeting from human to nonhuman characters. In *SIGGRAPH Asia 2023 Conference Papers*, pages 1–11, 2023. 3
- [32] C. Lu, X. Cheng, J. Li, S. Yang, M. Ji, C. Yuan, G. Yang, S. Yi, and X. Wang. Mobile-television: Predictive motion priors for humanoid whole-body control. *arXiv preprint arXiv:2412.07773*, 2024. 2, 3
- [33] N. Mahmood, N. Ghorbani, N. F. Troje, G. Pons-Moll, and M. J. Black. Amass: Archive of motion capture as surface shapes. In *Proc. of IEEE Conf. on Computer Vision and Pattern Recognition*, pages 5442–5451, 2019. 2
- [34] V. Makoviychuk, L. Wawrzyniak, Y. Guo, M. Lu, K. Storey, M. Macklin, D. Hoeller, N. Rudin, A. Allshire, A. Handa, et al. Isaac gym: High performance gpu-based physics simulation for robot learning. *arXiv preprint arXiv:2108.10470*, 2021. 3, 6
- [35] H. Miura and I. Shimoyama. Dynamic walk of a biped. *The International Journal of Robotics Research*, 3(2):60–74, 1984. 3
- [36] X. B. Peng, Z. Ma, P. Abbeel, S. Levine, and A. Kanazawa. Amp: Adversarial motion priors for stylized physics-based character control. *ACM Transactions on Graphics (TOG)*, 40(4):1–20, 2021. 6, 8
- [37] L. Peternel and J. Babič. Learning of compliant human–robot interaction using full-body haptic interface. *Advanced Robotics*, 27(13):1003–1012, 2013. 3
- [38] A. R. Punnakal, A. Chandrasekaran, N. Athanasiou, A. Quiros-Ramirez, and M. J. Black. Babel: Bodies, action and behavior with english labels. In *Proc. of IEEE Conf. on Computer Vision and Pattern Recognition*, pages 722–731, 2021. 2
- [39] S. Raab, I. Leibovitch, P. Li, K. Aberman, O. Sorkine-Hornung, and D. Cohen-Or. Modi: Unconditional motion synthesis from diverse data. In *Proc. of IEEE Conf. on Computer Vision and Pattern Recognition*, pages 13873–13883, 2023. 3
- [40] I. Radosavovic, T. Xiao, B. Zhang, T. Darrell, J. Malik, and K. Sreenath. Real-world humanoid locomotion with reinforcement learning. *Science Robotics*, 9(89):ead9579, 2024. 3
- [41] I. Radosavovic, B. Zhang, B. Shi, J. Rajasegaran, S. Kamat, T. Darrell, K. Sreenath, and J. Malik. Humanoid locomotion as next token prediction. In *Proc. of Advances in Neural Information Processing Systems*, 2024. 3
- [42] J. Ramos and S. Kim. Dynamic locomotion synchronization of bipedal robot and human operator via bilateral feedback teleoperation. *Science Robotics*, 4(35):eaav4282, 2019. 3
- [43] S. Ross, G. Gordon, and D. Bagnell. A reduction of imitation learning and structured prediction to no-regret online learning. In *Proceedings of the fourteenth international conference on artificial intelligence and statistics*, 2011. 6
- [44] J. Schulman, F. Wolski, P. Dhariwal, A. Radford, and O. Klimov. Proximal policy optimization algorithms. *arXiv preprint arXiv:1707.06347*, 2017. 4
- [45] S. Starke, I. Mason, and T. Komura. Deepphase: Periodic autoencoders for learning motion phase manifolds. *ACM Transactions on Graphics (TOG)*, 41(4):1–13, 2022. 3, 4
- [46] S. Tak and H.-S. Ko. A physically-based motion retargeting filter. *ACM Transactions on Graphics (ToG)*, 24(1):98–117, 2005. 3
- [47] R. Villegas, J. Yang, D. Ceylan, and H. Lee. Neural kinematic networks for unsupervised motion retargeting. In *Proc. of IEEE Conf. on Computer Vision and Pattern Recognition*, pages 8639–8648, 2018. 3
- [48] E. R. Westervelt, J. W. Grizzle, and D. E. Koditschek. Hybrid zero dynamics of planar biped walkers. *IEEE transactions on automatic control*, 48(1):42–56, 2003. 3
- [49] R. Yang, G. Yang, and X. Wang. Neural volumetric memory for visual locomotion control. In *Proc. of IEEE Conf. on Computer Vision and Pattern Recognition*, pages 1430–1440, 2023. 3

- [50] S. Yang, Z. Wu, M. Li, Z. Zhang, L. Hao, W. Bao, and H. Zhuang. Qpgesture: Quantization-based and phase-guided motion matching for natural speech-driven gesture generation. In *Proc. of IEEE Conf. on Computer Vision and Pattern Recognition*, pages 2321–2330, 2023. 3
- [51] K. Yin, K. Loken, and M. Van de Panne. Simbicon: Simple biped locomotion control. *ACM Transactions on Graphics (TOG)*, 26(3):105–es, 2007. 3
- [52] H. Zhao, H. Wang, C. Yang, and W. Shen. Chase: 3d-consistent human avatars with sparse inputs via gaussian splatting and contrastive learning. *arXiv preprint arXiv:2408.09663*, 2024. 2
- [53] H. Zhao, H. Wang, X. Zhao, H. Wang, Z. Wu, C. Long, and H. Zou. Automated 3d physical simulation of open-world scene with gaussian splatting. *arXiv preprint arXiv:2411.12789*, 2024. 2
- [54] H. Zhao, C. Yang, H. Wang, X. Zhao, and W. Shen. Sg-gs: Photo-realistic animatable human avatars with semantically-guided gaussian splatting. *arXiv preprint arXiv:2408.09665*, 2024. 2
- [55] C. Zheng and A. Vedaldi. Online clustered codebook. In *Proc. of IEEE Intl. Conf. on Computer Vision*, pages 22798–22807, 2023. 5
- [56] Z. Zhuang, S. Yao, and H. Zhao. Humanoid parkour learning. *arXiv preprint arXiv:2406.10759*, 2024. 3

SMAP : Self-supervised Motion Adaptation for Physically Plausible Humanoid Whole-body Control

Anonymous Author(s)

Affiliation

Address

email

1 A Real Robot System Setup

2 Our real robot is built on the Unitree H1 platform, as shown in Fig. 1, equipped with Damiao
3 DM-J4310-2EC motors. The control policy receives motion-tracking target information as input,
4 computes the desired joint positions for each motor, and sends commands to the robot’s low-level
5 interface. The policy’s inference frequency is set at 50 Hz. The commands are sent with a delay kept
6 between 18 and 30 milliseconds. The low-level interface operates at a frequency of 500 Hz, ensuring
7 smooth real-time control. The communication between the control policy and the low-level interface
8 is realized through LCM (Lightweight Communications and Marshalling).



Total weight: 47kg

Arm total length: 338 mm × 2 [4]

Thigh & shank length: 400 mm × 2 (each leg)

Battery: 15 Ah (0.864 kWh), Max voltage: 67.2 V

Key dimensions: (1520+285) mm × 570 mm × 220 mm

Joint torque limits (Knee): 360N·m

Joint torque limits (Hip): 220N·m

Joint torque limits (Ankle): 45N·m

Joint torque limits (Arm): 75N·m

Figure 1: **Details** about Unitree H1 robot.

9 B More Details of Humanoid Adapter

10 We then assume the two properties hold for the whole input sequence \mathbf{X} and extrapolate the phase
11 linearly with the predicted frequency to the whole sequence. We calculate the embeddings using
12 Eq. ??:

$$p = \Psi(\alpha, \phi) = \alpha^0 \sin(2\pi\phi) + \alpha^1 \cos(2\pi\phi), \quad (1)$$

13 with extrapolated phases and amplitudes. A decoder is then used to reconstruct the input motion
14 sequence from the predicted embedding. A decent reconstruction can only be achieved if the learned
15 mapping is close to phase linear and amplitude constant.

| Term | Expression | Weight |
|------------------------|--|------------|
| DoF acceleration | $\ \dot{d}_t\ _2^2$ | $-3e^{-7}$ |
| DoF position limits | $\mathbb{I}(d_t \notin [q_{\min}, q_{\max}])$ | -10 |
| DoF error | $\ d_t - d_0\ _2^2$ | -0.5 |
| Energy | $\ \tau_t \dot{d}_t\ _2^2$ | -0.001 |
| Linear velocity (z) | $\ v_t^{\text{lin-z}}\ _2^2$ | -1 |
| Angular velocity (xy) | $\ v_t^{\text{ang-xy}}\ _2^2$ | -0.4 |
| Action rate | $\ a_t - a_{t-1}\ _2^2$ | -0.1 |
| Torque | $\ \tau_t\ _2$ | -0.0001 |
| Feet air time | $T_{\text{air}} - 0.5$ | 10 |
| Feet velocity | $\ v_{\text{feet}}\ _1$ | -0.1 |
| Feet contact force | $\ F_{\text{feet}}\ _2^2$ | -0.003 |
| Stumble | $\mathbb{I}(F_{\text{feet}}^x > 5 \times F_{\text{feet}}^z)$ | -2 |
| Hip pos error | $\ p_t^{\text{hip}} - p_0^{\text{hip}}\ _2^2$ | -0.2 |
| Waist roll pitch error | $\ p_t^{\text{wrp}} - p_0^{\text{wrp}}\ _2^2$ | -1 |
| Ankle Action | $\ a_t^{\text{ankle}}\ _2^2$ | -0.1 |

Table 1: **Regularization rewards** Regularization rewards for preventing undesired behaviors for sim-to-real transfer.

| Term | Expression | Weight |
|---------------------------|--|--------|
| DoF Position (Upper) | $\exp(-0.7\ \mathbf{q}_{ref}^{\text{upper}} - \mathbf{q}^{\text{upper}}\)$ | 3.0 |
| DoF Position (Lower) | $\exp(-0.7\ \mathbf{q}_{ref}^{\text{lower}} - \mathbf{q}^{\text{lower}}\)$ | 1.0 |
| Keypoint Position (Upper) | $\exp(-\ \mathbf{p}_{ref}^{\text{upper}} - \mathbf{p}^{\text{upper}}\)$ | 2.0 |
| Keypoint Position (Lower) | $\exp(-\ \mathbf{p}_{ref}^{\text{lower}} - \mathbf{p}^{\text{lower}}\)$ | 1.0 |
| Linear Velocity | $\exp(-4.0\ \mathbf{v}_{ref} - \mathbf{v}\)$ | 6.0 |
| Velocity Direction | $\exp(-4.0 \cos(\mathbf{v}_{ref}, \mathbf{v}))$ | 6.0 |
| Roll & Pitch | $\exp(-\ \boldsymbol{\Omega}_{ref}^{\phi\theta} - \boldsymbol{\Omega}^{\phi\theta}\)$ | 1.0 |
| Yaw | $\exp(- \Delta y)$ | 1.0 |

Table 2: **Tracking Reward.** $\mathbf{q}_{ref}^{\text{upper/lower}}$ and $\mathbf{p}_{ref}^{\text{upper/lower}}$ denote the reference joint and keypoint positions for the upper and lower body, respectively. \mathbf{v}_{ref} is the reference velocity of the body, while $\boldsymbol{\Omega}_{ref}^{\phi\theta}$ and $\boldsymbol{\Omega}^{\phi\theta}$ denote the reference and actual roll and pitch of the body.

The encoder uses a 2-layer 1D convolutional network to map the input to an intermediate representation, which is then split into two branches: the timing branch and the amplitude branch. The timing branch predicts phase ϕ and frequency f from a temporal signal generated by a 1D convolution, while the amplitude branch predicts amplitude \mathbf{A} by applying average pooling followed by an MLP, with vector quantization used to select the nearest amplitude from a finite codebook.

The phase is calculated using the relative timing \mathcal{T} and the equation $\Phi = \phi + f \cdot \mathcal{T}$. The final motion embedding is obtained by $\mathbf{P} = \Psi(\mathbf{A}, \Phi)$. The decoder is a 2-layer 1D convolutional network that maps the embedding back to the original motion space.

C More Details of Reward

In the main paper, we introduce the tracking reward. Tab. 1 and Tab. 2 shows details on the regularization reward.

D More Details of Observation of RL

The student policy’s observation comprises the following components: Base angular velocity, IMU measurements (roll and pitch angles), Directional difference between current yaw angle and target yaw (represented as sine and cosine terms), Joint positions and velocities, Observation history from the past n steps, and Target goal.

| Codebook size | E_{mpkpe} |
|---------------|-------------|
| 16 | 12.3 |
| 32 | 10.6 |
| 64 | 10.7 |

Table 3: Mean per joint position error (cm) of Humanoid-Adapter.

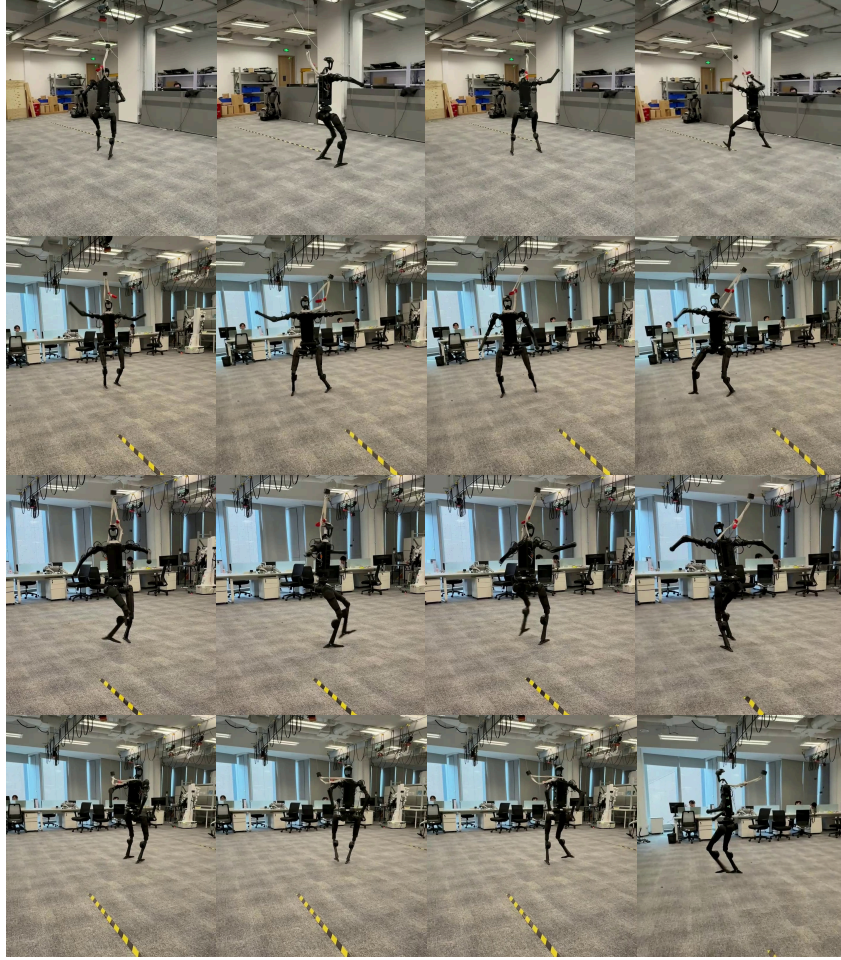


Figure 2: Expressive motion evaluation in the real world..

32 The teacher policy’s observation extends the student policy’s observation with privileged information,
33 including: Foot contact flags, System dynamics parameters (mass, ground friction coefficients, motor
34 strength parameters), External push forces.

35 E Performance of Humanoid-Adapter

36 We save a set of paired human motion and humanoid robot motion data (saved by simulator with a
37 RL policy) to evaluate the performance of our Humanoid-Adapter, as shown in Tab. 3.

38 F Additional Real World Results Visualization

39 We provide detailed visualization for some motions evaluated in the real world in Fig. 2.